



**HAL**  
open science

# Characterization of High-Temperature Superconductor Bulks for Electrical Machine Application

Bruno Douine, Kévin Berger, Nickolay Ivanov

► **To cite this version:**

Bruno Douine, Kévin Berger, Nickolay Ivanov. Characterization of High-Temperature Superconductor Bulks for Electrical Machine Application. *Materials*, 2021, 14 (7), pp.1636. 10.3390/ma14071636 . hal-03183546

**HAL Id: hal-03183546**

**<https://hal.univ-lorraine.fr/hal-03183546>**

Submitted on 27 Mar 2021

**HAL** is a multi-disciplinary open access archive for the deposit and dissemination of scientific research documents, whether they are published or not. The documents may come from teaching and research institutions in France or abroad, or from public or private research centers.

L'archive ouverte pluridisciplinaire **HAL**, est destinée au dépôt et à la diffusion de documents scientifiques de niveau recherche, publiés ou non, émanant des établissements d'enseignement et de recherche français ou étrangers, des laboratoires publics ou privés.



Distributed under a Creative Commons Attribution 4.0 International License

Review

# Characterization of High-Temperature Superconductor Bulks for Electrical Machine Application

Bruno Douine <sup>1,\*</sup>, Kevin Berger <sup>1</sup> and Nickolay Ivanov <sup>2</sup>

<sup>1</sup> Groupe de Recherche en Energie Electrique de Nancy (GREEN), Université de Lorraine, Vandoeuvre-lès-Nancy 54506, France; kevin.berger@univ-lorraine.fr

<sup>2</sup> Moscow Aviation Institute (MAI), Moscow 125993, Russia; n.s.ivanov88@gmail.com

\* Correspondence: bruno.douine@univ-lorraine.fr

**Abstract:** High-temperature superconducting (HTS) bulks can be used in electrical applications. Experimental characterization of large-size HTS bulks is a tricky issue. The relevant parameters for their application were directly measured in this study. This paper has three main aims. Firstly, features of YBaCuO bulks are presented. Secondly, an electrical motor application is developed using magnetic field shielding and trapping. Thirdly, the HTS bulks are characterized. Several classical methods were used, which are mainly magnetic methods only available for small samples. The complete penetration magnetic field and the critical current density were found to be the main parameters relevant for applications. An innovative entire HTS bulk characterization method is presented. This characterization method is useful for end users and engineers to better implement HTS bulks.

**Keywords:** high-temperature superconductor; characterization; electrical motor

**Citation:** Douine, B.; Berger, K.; Ivanov, N. Characterization of High Temperature Superconductor Bulks for Electrical Machine Application. *Materials* **2021**, *14*, 1636. <https://doi.org/10.3390/ma14071636>

Academic Editor: Pavel Diko

Received: 10 February 2021

Accepted: 22 March 2021

Published: 26 March 2021

**Publisher's Note:** MDPI stays neutral with regard to jurisdictional claims in published maps and institutional affiliations.



**Copyright:** © 2021 by the authors. Licensee MDPI, Basel, Switzerland. This article is an open access article distributed under the terms and conditions of the Creative Commons Attribution (CC BY) license (<http://creativecommons.org/licenses/by/4.0/>).

## 1. Introduction

High-temperature superconducting (HTS) bulks can be used in electrical applications as magnets or magnetic shields. Indeed, they have a high critical current density  $J_c$  and can be magnetized to very high magnetic flux densities. The main applications of HTS bulks are levitation, cryo-magnets, electrical motors, and magnetic gears.

It is necessary to characterize this HTS bulks to optimally use them. This means the determination of the critical current density  $J_c$ . Different classical methods have been used for small samples [1–21]. The goal of these classical methods is mainly to obtain the dependence of  $J_c$  on the magnetic field  $B$  and temperature of the HTS material. Different characterization methods exist, such as magnetization methods, measurements of susceptibility, or measurements of levitation force. In these classical characterization methods, the relationship between measurements and  $J_c$  is not direct and, thus, these are called indirect methods. On another hand, Mawatari [9,10] proposed using an electric characterization method to characterize HTS bulks, by cutting a strip in the HTS bulk. This allows directly determining  $J_c$ , but it modifies the properties of the HTS sample in comparison with the entire HTS bulk. The main issue with these characterization methods is that there are valid only for small samples cut into entire HTS bulks. This is sufficient for material scientists and it allows comparing HTS materials, but it is not useful for applications. End users of HTS bulks, such as engineers or electrical engineering researchers, need characterization of the entire HTS bulks to optimally use them in applications. Hence, for real HTS bulks used in electrical applications, other methods are necessary, allowing characterization of the entire HTS bulks without cutting. Recently, the CAN company [8], building and selling HTS YBaCuO bulks, proposed characterizing different samples of HTS material placed at different regions in the YBaCuO bulk to better

characterize their products. This proves that companies need a characterization method for entire HTS bulk. This kind of characterization method is at the boundary between material scientists, companies, and engineers. Previously, Vanderbemden [17] used pick up coils and Hall probes to characterize entire HTS bulks with a magnetization cycle. In the last few last years, we proposed a new direct magnetic determination method for  $J_c$  and  $n$ -value. It consists of the determination of the complete penetration magnetic field  $B_p$  and a deduction of the critical current density  $J_c$ . This new method is original, quick, and direct for determining the critical current density  $J_c$  and  $n$ -value in bulk superconductors from magnetic field diffusion measurements [18–21]. Experimental characterization of large-size samples is a tricky issue. This process is considered an “engineering characterization” of the HTS bulks used in application. Thus, the relevant parameters, such as the complete penetration magnetic field, for applications should be directly measured.

This paper has three main aims. Firstly, features of YBaCuO bulks are presented and compared with respect to applications. Secondly, an HTS electrical motor application is presented. Lastly, the innovative HTS bulk characterization method is described.

## 2. High-Temperature Superconducting Bulks

### 2.1. Composition of HTS Bulks

HTS bulks are composed of copper-oxide layers and a rare earth element as Yttrium [22]. The superconductivity exists in the  $a$ - $b$  plane of the copper-oxide layer. In the  $c$ -direction, perpendicular to the  $a$ - $b$  plane, the electric conductivity is close to zero. Thus, HTS materials are clearly anisotropic.

The HTS bulks used for applications as motors or super magnets are mono crystals. More than 20 years ago, top-seeded melt growth (TSMG) was established, which allowed building large, single-grain HTS bulks [23]. The process of HTS bulk fabrication is the growing of one mono crystal from a seed at the center of the HTS bulk. Figure 1 shows the seed at the center of HTS bulks. These materials have significant potential for application as high-field permanent magnets. The performance of these magnets at 77 K is limited by the critical current carrying capacity of the bulk superconductor. The values of  $J_c$  are more than 100 A/mm<sup>2</sup> at 77 K, and the size can be more than 5 cm diameter (Figure 1) with different shapes.



**Figure 1.** Mono crystal high-temperature superconducting (HTS) bulks from ATZ company.

### 2.2. Critical Quantities

As a superconducting material, HTS bulks have three critical quantities: critical temperature  $T_c$  (92 K for YBaCuO), critical current density  $J_c$ , and critical magnetic field  $H_c$ . Because HTS materials are used at high temperature ( $T > 30$  K), there is another important magnetic field, called the irreversibility magnetic field  $H^*$ , between  $H_{c1}$ , where the penetration of the magnetic field begins, and  $H_{c2}$ , where the superconductivity disappears. If the magnetic field inside the HTS material is higher than this irreversibility magnetic field, the critical current density drops to zero. Thus,  $H^*$  is the most important magnetic field parameter to know for electric applications as motors, because, in this case,

a high electric current density and high magnetic field are simultaneously necessary to improve motor capability and efficiency.

### 3. HTS Bulk Application in Electrical Machines

HTS bulk can be used as a magnetic shield or permanent magnet in superconducting electrical machines.

#### 3.1. Magnetic Flux Concentration Machines from GREEN Lab

GREEN lab in France designed, built, and tested many HTS machines using a magnetic shield producing a magnetic field concentration.

The inductor of the first prototype built in GREEN was originally presented in [24]. It used the high capacity of two superconducting coils (Figure 2) to produce a high magnetic field without iron (Figure 2) and the magnetic shielding of HTS bulks. The two superconducting coils create two magnetic fields in opposition, which create a high radial magnetic field between them. The HTS bulks used as magnetic field shields create spatial variation of the magnetic field along the perimeter of the inductor. This spatial variation can be used to generate alternating current (AC) voltage in induced part coils or to produce torque between this inductor and induced part. HTS materials enable reaching levels of magnetic flux density much higher than those obtained using classic magnetic materials. This prototype (Figure 3) was built and tested on the basis of this principle [25]. The coils of the induced part were made with copper because only the inductor was cooled down at the temperature of liquid helium. Liquid helium was chosen as the cooling system because it is a simple solution to cool down the NbTi coils producing a high magnetic field, which ensures that the HTS bulks perfectly shield this high magnetic field. Actually, a higher temperature reduces the magnetic shielding of the HTS bulks because the penetration depth of the magnetic field inside the HTS bulk depends on the critical current density  $J_c$ , which decreases when temperature increases.

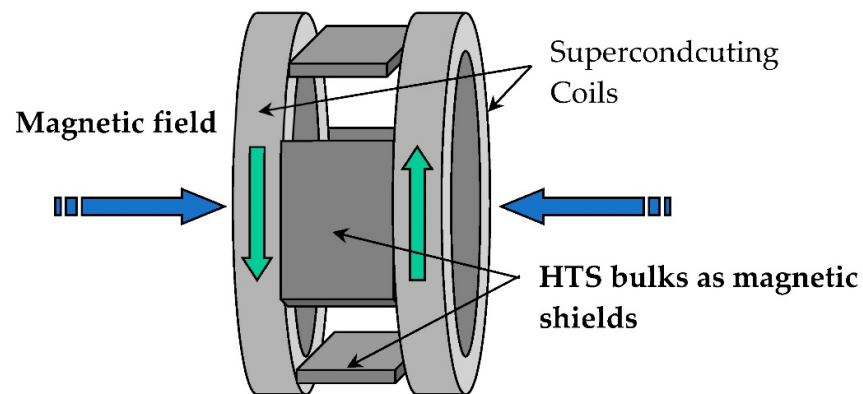


**Figure 2.** Inductor of the motor with HTS bulk magnetic flux concentration.

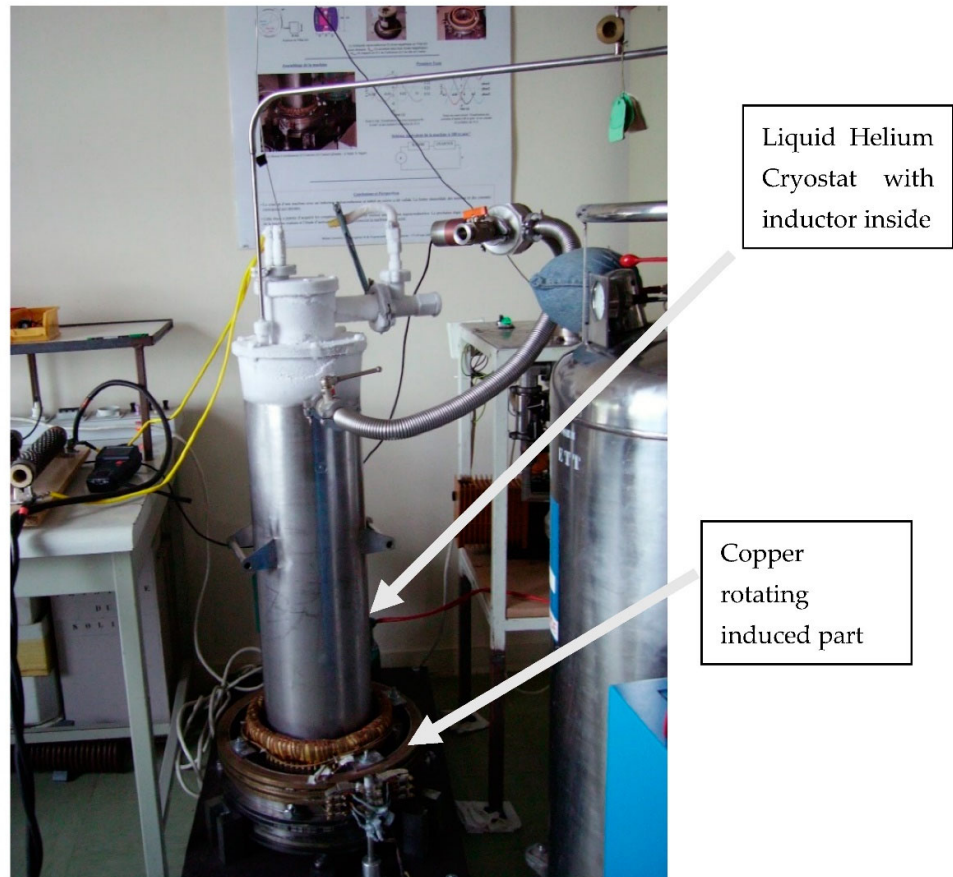


**Figure 3.** HTS bulk magnetic flux concentration inductor motor.

Following this first machine, a collaboration began a few years ago between SAFRAN and GREEN to construct an HTS motor for aeronautic applications (Figure 4).

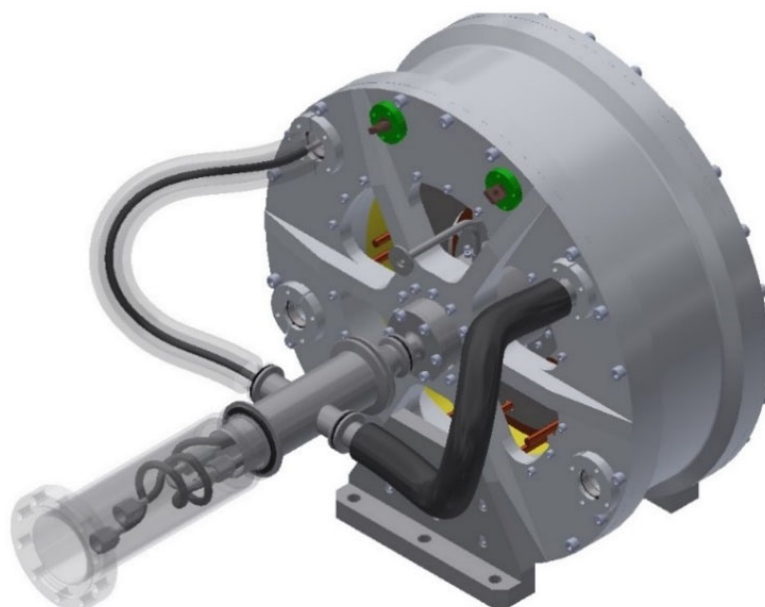


**Figure 4.** HTS motor from GREEN and SAFRAN for aeronautic applications.

In this second magnetic flux concentration motor [26], the HTS coil produces a high axial magnetic field, and five HTS pellets, which rotate, shield the magnetic field and concentrate the magnetic field between them. The armature is made with copper winding at room temperature, because the AC losses would be too high at low temperature (Figure 5). This motor is under patent, thus, further details are classified.

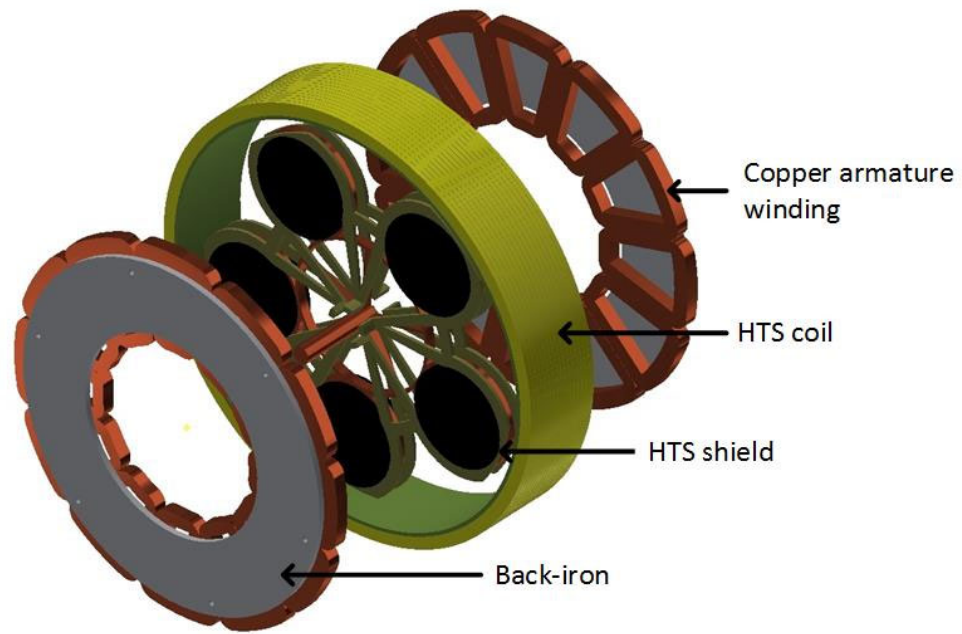


**Figure 5.** HTS coils producing an axial magnetic field, with HTS bulks as a magnetic shield and armature windings.

### 3.2. HTS Permanent Magnet Machine

The HTS YBaCuO bulk, submitted to a magnetic field and then cooled down, traps the magnetic field. This method is called zero field cooling (ZFC). It is possible to obtain 4 T on the surface of a YBaCuO bulk at 77 K (liquid nitrogen) and up to 17 T at 29 K [27] and 17.9 T at 26 K [23]. The ZFC method takes time and a huge superconducting coil. Thus, magnetization of HTS bulks is not suitable for motor applications. A suitable magnetization method exists called pulse field magnetization (PFM). In this method, the HTS YBaCuO bulk is cooled down and then submitted to magnetic field pulses [28–30]. It traps less of the magnetic field than the ZFC method but it requires only a small copper magnetization coil. It allows the production of prototypes where HTS bulks on a rotor are magnetized and used as permanent magnets. In Japan, Professor Izumi and his team have been working on this topic for many years, and they have built several prototypes [31–33]. In England, Dr. Coombs has also built a prototype [34](Figure 6).

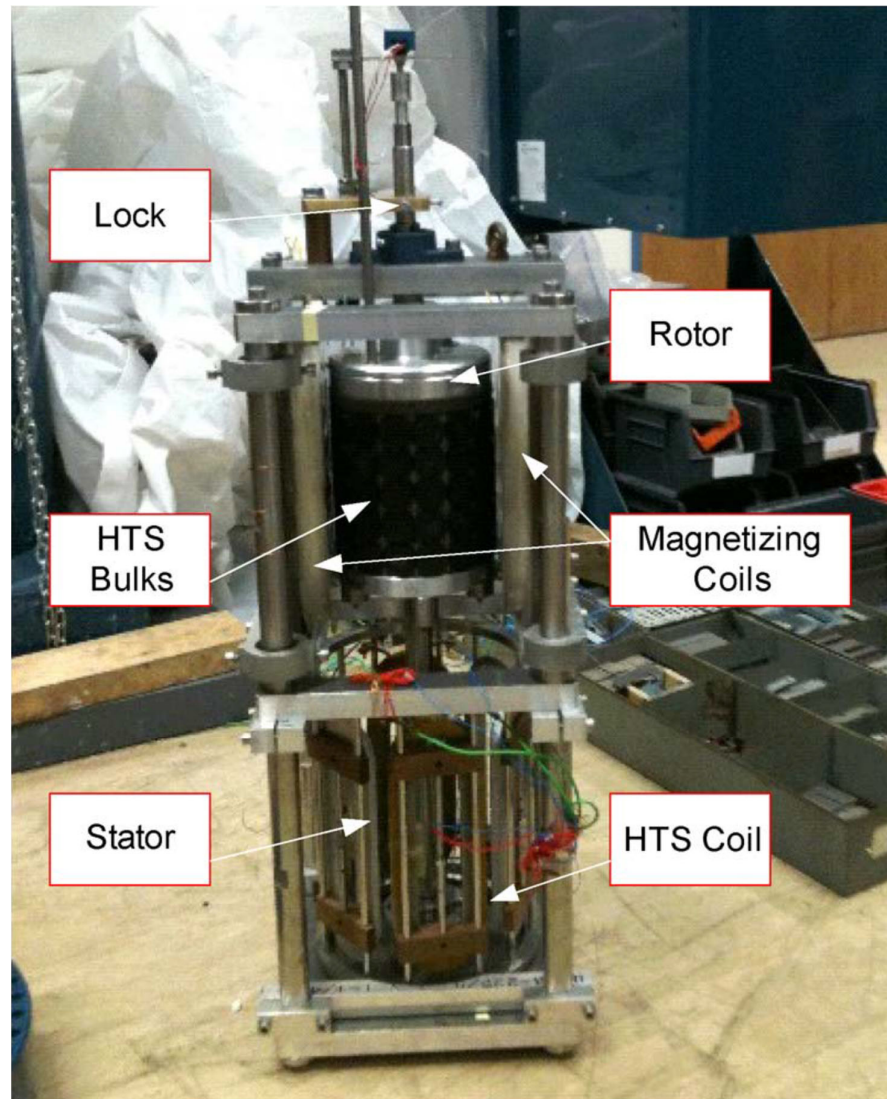


**Figure 6.** HTS bulk motor designed and built by Dr Coombs et al. [34].

One of the issues with this kind of HTS motor is the choice of whether to magnetize the HTS bulks inside the machine (in situ) or outside of the machine (ex situ). The prototypes already made used ex situ magnetization because it is the simplest option in terms of magnetization. However, many teams [28–31] are working on in situ magnetization for future industrial applications because it should be simpler for the end user.

Trapping the magnetic field in the HTS bulk using the PFM method depends on the critical current density  $J_c$ , the size of the HTS bulk, and the form of the applied magnetic field pulse [28–30]. In a synchronous HTS motor, the HTS bulks replace permanent magnets. Figure 7 presents a simplified model of the magnetic circuit with an HTS bulk plug on the rotor of an electrical machine. Field lines are in the air, iron, and superconducting bulk. GREEN lab studied the magnetization of HTS bulk in an iron core (Figure 7), and they concluded that the trapped magnetic field in the HTS bulk increased and the current of the optimal pulse decreased. Therefore, iron around the HTS bulk improved the magnetization process [29,30].

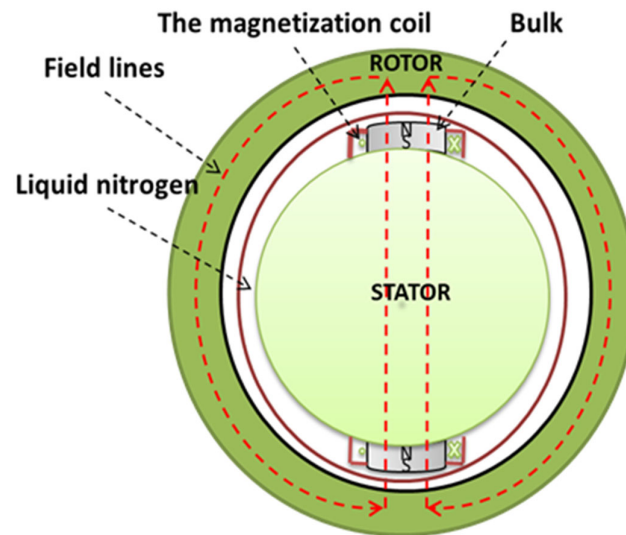


Figure 7. Simplified magnetic circuit of HTS bulk motor.

#### 4. Characterization of HTS Bulks

In this section, the HTS bulk characterization method developed by us is presented; however, the complete penetration magnetic field is firstly defined.

##### 4.1. Definition of the Complete Penetration Magnetic Field $B_p$

The most used definition of the complete penetration magnetic field  $B_p$  is generally linked to the Bean model [1]. In this model, the current density is assumed equal to the critical current density  $J_c$  or null in the superconducting material. With this model, the penetration depth  $d_p$  of the magnetic field in a superconducting infinite cylinder submitted to an axial applied magnetic field  $B_a$  is calculated as

$$d_p = \frac{B_a}{\mu_0 J_c}. \quad (1)$$

Therefore, if the magnetic field reaches the center of the infinite cylinder, where  $d_p = R$  is the radius of the cylinder, the complete penetration magnetic field is defined by

$$B_p = \mu_0 J_c R. \quad (2)$$

For electrical motor applications using HTS bulk, the penetration depth  $d_p$ , related to  $J_c$ , allows determining the capability of magnetic shielding. On the other hand, the complete penetration magnetic field  $B_p$  allows determining the capability of magnetic field trapping of HTS bulks.

The shape of  $B_a(t)$  does not matter with the Bean model; hence, we applied the following equation:

$$B_a(t) = V_b \cdot t. \quad (3)$$

At the center of the HTS bulk, the magnetic field  $B_0$  begins to increase with delay time  $T_p$  when  $B_a$  reaches the complete magnetic field  $B_p$  (Figure 8).



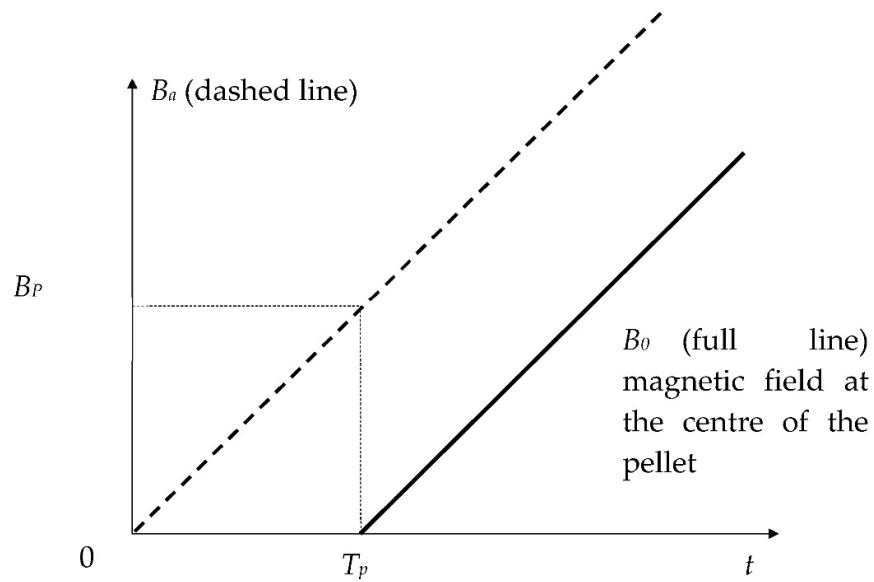


**Figure 8.** Applied magnetic field  $B_a(t)$  and magnetic induction at the center of the cylindrical HTS bulk  $B_o(t)$ .

For a cylindrical HTS bulk of length  $L$  and radius  $R$ , submitted to an applied magnetic field  $B_a(t)$  (Figure 9), the following explicit expression of the penetration magnetic field  $B_p$  can be calculated using the Bean model [32]:

$$B_p = \frac{\mu_0 J_c \cdot L}{4} \cdot \ln \left( \frac{\sqrt{R^2 + \left(\frac{L}{2}\right)^2} + R}{\sqrt{R^2 + \left(\frac{L}{2}\right)^2} - R} \right), \tag{4}$$

where  $L$  is the length of the cylinder and  $R$  is its radius. Equation (2) is the equivalent of the  $B_p$  formula given by different authors [18–21].

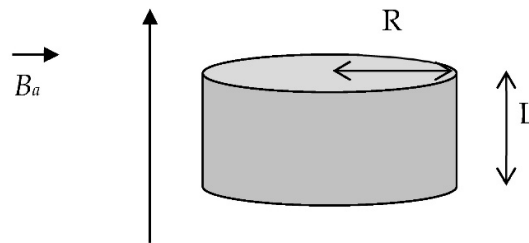


**Figure 9.** A cylindrical HTS bulk with its axis parallel to the applied magnetic field.

Thus, from  $B_p$  and the geometric parameters of the cylindrical HTS pellet,  $J_c$  can be deduced with the help of Equation (4).

In the case of HTS used at “high temperatures” (typically above 50–60 K), a power law model (PLM) better represents the  $E(J)$  characteristic of the materials than the Bean model. The PLM is typically written as

$$E = E_c \left( \frac{J}{J_c} \right)^n = \frac{E_c}{J_c} \left( \frac{J}{J_c} \right)^{n-1} J. \tag{5}$$

The determination of  $B_p$ ,  $J_c$ , and  $n$ -value of HTS bulks can be done by measurement and numerical simulation of magnetic field penetration [19]. The influence of the rise rate of the applied magnetic field  $V_b$  changes the distribution of the magnetic field and current

density according to the power law (Equation (5)) instead of the Bean model [17]. Thus,  $B_P$  depends on the rise rate  $V_b$  as follows:

$$B_P = \frac{\mu_0 J_C \cdot L}{4} \cdot \ln \left( \frac{\sqrt{R^2 + \left(\frac{L}{2}\right)^2} + R}{\sqrt{R^2 + \left(\frac{L}{2}\right)^2} - R} \right) \left( 1 + \frac{\alpha \ln V_b + \beta}{n} \right), \quad (6)$$

where  $\alpha = 1.2$  and  $\beta = 3.4$  for a typical HTS bulk size.

#### 4.2. Presentation of the Characterization Method

In this method, the HTS sample is submitted to an axial applied magnetic field  $B_a(t)$  (Figure 8).  $B_a(t)$  is a linear function of time. In our method, the complete penetration magnetic field is detected. To measure  $B_P$  [18–20], an axial Hall probe, placed between two identical cylindrical HTS bulks (Figure 10) at their center, detects the penetration of the magnetic field. Theoretically, these two pellets are considered as one unique pellet. Therefore, the influence of the Hall probe thickness  $e$  is neglected. At the position of the Hall probe, the magnetic field has only an axial component; thus, the magnetic field can be well measured with this axial Hall probe. In our experiment (Figure 11), the applied magnetic field  $B_a(t)$  had a constant rise rate  $V_b$  of  $\sim 660$  T/s. As shown in the red region of Figure 11, the beginning of  $B_o(t)$  does not have exactly the same shape as the beginning of  $B_a(t)$ . This is due to the fact that this is not a single HTS bulk but two bulks separated by the Hall probe thickness. The influence of the thickness of the Hall probe  $e$  is presented below. The determination of the penetration time  $T_P$  is done as follows: the measured magnetic field curve at the pellet center is modified around  $T_P$  to be a copy of applied magnetic field  $B_a(t)$  (dotted line in Figure 11). Throughout time, the difference between curves is constant and equal to  $T_P$ .  $T_P$  is determined, and then  $B_P$  can be deduced from the curves.

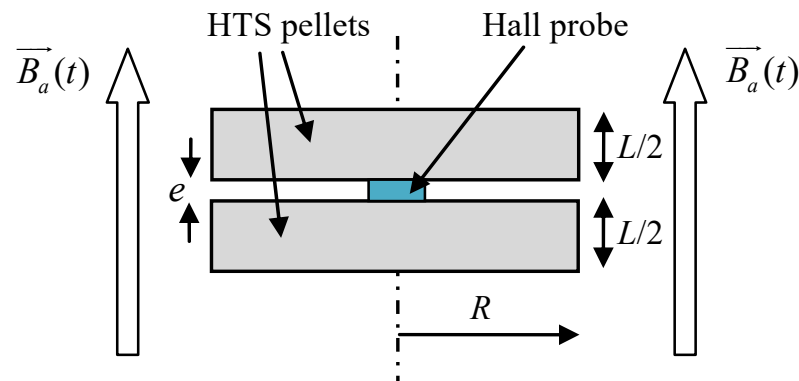


**Figure 10.** Hall probe location between two HTS bulks.

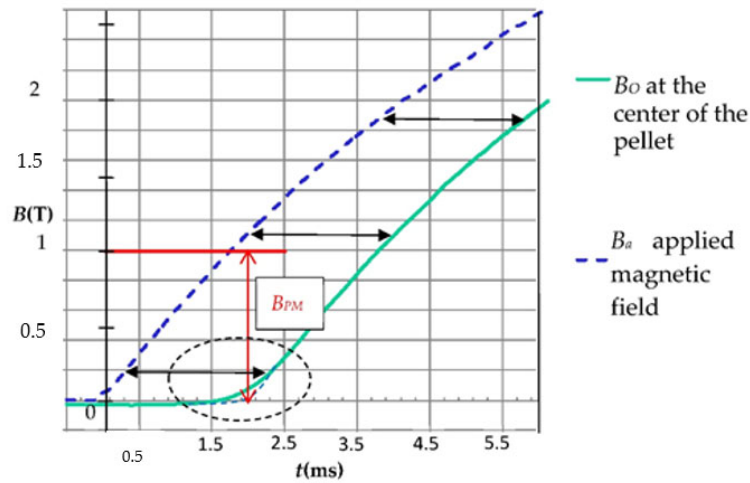


**Figure 11.** Applied magnetic field  $B_a$  and measured magnetic field  $B_0$  at the center of the HTS bulk versus time.

The influence of Hall probe thickness  $e$  (Figure 10) was calculated with the help of a numerical simulation [19]. The thickness of the Hall probe  $e$  was around 0.5 mm. The relationship between the measured complete penetration magnetic field  $B_{PM}$  and the theoretical  $B_P$  from (Equation (6)) is as follows:

$$\frac{B_{PM}}{B_P}(e = 0.5 \text{ mm}) = 0.031 \ln(L) + 0.82. \quad (7)$$

For the two YBaCuO bulks presented in Figure 11, the measured  $B_{PM}$  was around 1 T (red arrow).  $B_P$  was deduced from  $B_{PM}$  using Equation (7) and knowing  $e$  and  $L$ .  $J_c$  was deduced from  $B_P$  with Equation (6) and with  $n$  taken as equal to 50, giving a result of  $\sim 110$  A/mm<sup>2</sup>.

This method has two main limitations. Firstly, it requires two identical HTS bulks. Secondly, the position of the seeds of the two HTS bulks modifies the results of  $B_{PM}$  and the  $J_c$  determination, as shown in Figure 12 and Table 1. In Figure 12, different positions of the seeds in relation to each HTS bulk were tested in the GREEN lab. The results of  $B_{PM}$  (Table 1) were different for each case. This is because of the inhomogeneity of the HTS bulk. The value of  $J_c$  is bigger close to the seed and smaller far from the seed. A more complex model of the HTS bulk is necessary to consider its inhomogeneity. We propose a model with three critical current density values across three regions. In Figure 13, the HTS bulk of radius  $R$  and length  $L$  is decomposed in three regions. Region I is a cylinder with a top seed of radius  $R/3$  and length  $L/3$ . Region II is a cylinder of radius  $2R/3$  and length  $2L/3$  excluding region I. Region III is the cylindrical HTS bulk excluding region I and II. The critical current in region I (radius is bigger than in region II and much bigger than in region III). This decomposition into three regions allows refining the characterization method by mixing new experimental results and numerical simulations. We expect to improve our characterization method using this new model.

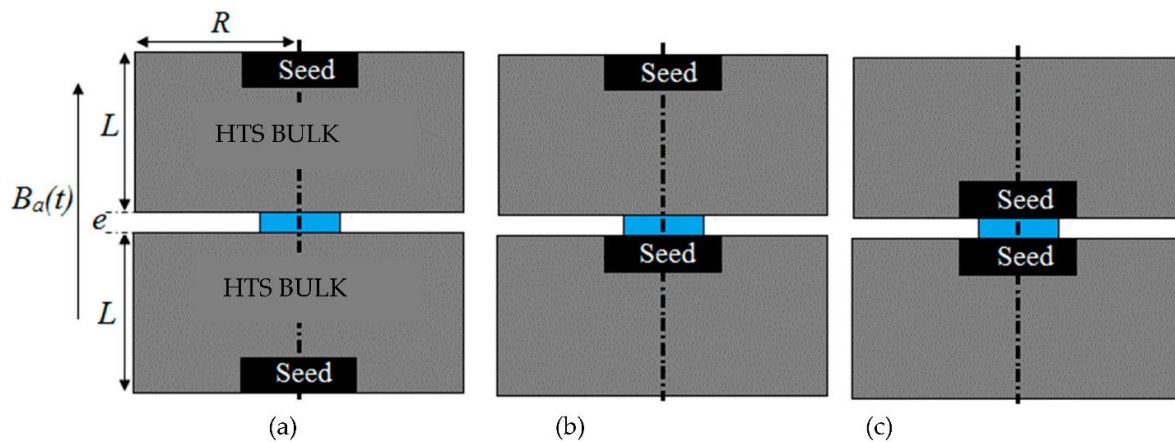


**Figure 12.** Different positions of the HTS bulk seeds (in black) in relation to the Hall probe (in blue). For case (a) the two seeds far from the Hall probe, case (b) one seed far from the Hall probe and one seed close to the Hall probe and case (c) the two seeds close to the Hall probe.

**Table 1.** Measurements of  $T_P$  and  $B_{PM}$  for the three cases (a), (b), and (c).

|                      | Case (a) | Case (b) | Case (c) |
|----------------------|----------|----------|----------|
| $T_P$ ( $10^{-3}$ s) | 0.93     | 1.32     | 1.4      |
| $B_{PM}$ (T)         | 2.57     | 3.02     | 3.1      |

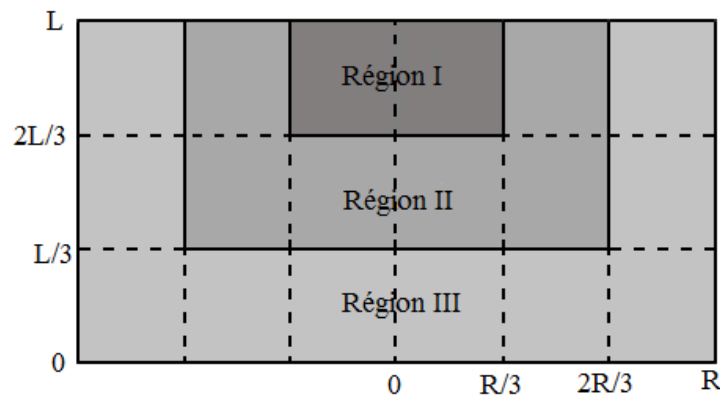


**Figure 13.** Model of HTS bulk considering homogeneity.

## 5. Conclusions

HTS bulks are very promising for electrical motor applications as super magnets or magnetic shields. HTS bulks are built and sold by industrial companies. Electrical motor prototypes were built and successfully tested by different teams using a shielding effect and HTS permanent magnets. The magnetization and characterization of these HTS bulks are necessary to control their use in electrical motor applications. A new direct  $J_c$  determination method is presented based on the measurement of  $B_p$ . It is a relatively precise method, while it importantly considers the rise rate and Hall probe thickness. It is a valid method to quickly obtain a rough value of  $J_c$  for HTS bulk. However, this method does not determine  $J_c(B)$ ; as such, improvements will be necessary.

**Author Contributions:** Conceptualization, B.D., K.B. and N.I.; methodology, B.D.; software, K.B.; validation, B.D., K.B. and N.I.; formal analysis, B.D.; investigation, B.D.; resources, B.D., K.B. and N.I.; data curation, B.D., K.B. and N.I.; writing—original draft preparation, B.D.; writing—review and editing, B.D.; visualization, B.D., K.B. and N.I.; supervision, B.D.; project administration, B.D.;

funding acquisition, B.D., K.B. and N.I. All authors have read and agreed to the published version of the manuscript.

**Funding:** The study was carried out with the financial support of a project by the Russian Federation represented by the Ministry of Education and Science of the Russian Federation, agreement N°075-15-2020-770.

**Institutional Review Board Statement:** Not applicable.

**Informed Consent Statement:** Not applicable.

**Data Availability Statement:** Not applicable.

**Conflicts of Interest:** The authors declare no conflict of interest.

**Conflicts of Interest:** The authors declare no conflict of interest.

## References

1. Bean, C.P. Magnetization of high-field superconductors. *Rev. Mod. Phys.* **1964**, *36*, pp. 31–39.
2. Kim, Y.B.; Hempstead, C.F.; Strnad, A.R. Critical persistent currents in hard superconductors. *Phys. Rev. Lett.* **1962**, *9*, pp. 306–309.
3. Hulbert, J.A. Magnetization of a cylindrical hard superconductor. *Br. J. Appl. Phys.* **1965**, *16*, pp. 1657–1666.
4. Sanchez, A.; Navau, C. Critical current density from magnetization loops of finite high-TC superconductors. *Supercond. Sci. Technol.* **2001**, *14*, pp. 444–447.
5. Shantsev, D.V.; Galperin, Y.M.; Johansen, T.H. Thin superconducting disk with B-dependent  $J_c$ : Flux and current distributions. *Phys. Rev. B* **1999**, *60*, 13112–13118.
6. Chen, D.X.; Goldfarb, R.B. Kim model magnetization of type II superconductors. *J. Appl. Phys.* **1989**, *66*, 2489–2500.
7. Antal, V.; Volochová, D.; Kavečanský, V.; Kováč, J.; Diko, P. Influence of annealing in oxygen and argon on the superconducting properties of Li-doped YBCO single-grain bulks. *Physica C* **2017**, *541*, pp. 22–29.
8. Antal, V.; Zmorayová, K.; Rajnak, M.; Vojtková, L.; Hlášek, T.; Plecháček, J.; Diko, P. Relationship between local microstructure and superconducting properties of commercial YBa<sub>2</sub>Cu<sub>3</sub>O<sub>7-δ</sub> bulk. *Supercond. Sci. Technol.*, **2020**, , 33, 044004.
9. Mawatari, Y.; Sawa, A.; Obara, H.; Umeda, M.; Yamasaki, H. Field-sweep rate dependence of magnetization and current-voltage characteristics in superconducting disks. *Appl. Phys. Lett.* **1997**, *70*.
10. Yamasaki, H.; Mawatari, Y. Current voltage characteristics and flux creep in melt-textured YBaCuO. *Supercond. Sci. Technol.* **2000**, *13*, pp. 202–208.
11. Vanderbemden, P.; Misson, V.; Ausloos, M.; Cloots, R. Magnetic and transport measurements on melt-textured DyBCO single domains. *Physica C* **2002**, *372–376*, 1225–1228.
12. Senoussi, S. Review of the critical current densities and magnetic irreversibilities in high T<sub>c</sub> superconductors. *J. Phys. III* **1992**, *2*, 1041–1257.
13. Douine, B.; Leveque, J.; Mezani, S.  $J_c(B)$  determination method with the help of the virgin magnetization curve of a superconducting cylinder. *IEEE Trans. Appl. Supercond.* **2010**, *20*, 82–86.
14. Chen, D.X.; Brug, J.A.; Goldfarb, R.B. Demagnetizing factors for cylinders. *IEEE Trans. Magn.* **1991**, *27*, 3601–3619.
15. Sanchez, A.; Navau, C. Influence of demagnetizing effects in superconducting cylinders. *IEEE Trans. Appl. Supercond.* **1999**, *9*, 2195–2198.
16. Sanchez, A.; Navau, C. Magnetic properties of finite superconducting cylinders, uniform applied field. *Phys. Rev. B* **2001**, *64*, 214506.
17. Philippe, M.P.; Fagnard, J.-F.; Kirsch, S.; Xu, Z.; Dennis, A.R.; Shi, Y.-H.; Cardwell, D.A.; Vanderheyden, B.; Vanderbemden, P. Magnetic characterisation of large grain, bulk Y-Ba-Cu-O superconductor-soft ferromagnetic alloy hybrid structures. *Physica C* **2014**, *502*, 20–30.
18. Douine, B.; Sirois, F.; Leveque, J.; Berger, K.; Bonnard, C.H.; Hoang, T.C.; Mezani, S. A New Direct Magnetic Method for Determining  $J_c$  in Bulk Superconductors from Magnetic Field Diffusion Measurements. *IEEE Trans. Appl. Supercond.* **2012**, *22*, 9001604.
19. Douine, B.; Bonnard, C.H.; Sirois, F.; Berger, K.; Kameni, A.; Lévêque, J. Determination of  $J_c$  and n-value of HTS Pellets by Measurement and Simulation of Magnetic Field Penetration. *IEEE Trans. Appl. Supercond.* **2015**, *25*, 8001008.
20. Douine, B.; Berger, K.; Bonnard, C.H.; Sirois, F.; Kameni, A.; Lévêque, J. Improved Method for determining the n-value of HTS bulks. *IEEE Trans. Appl. Supercond.* **2016**, *26*, 6800704.
21. Douine, B.; Berger, K.; Trillaud, F.; Elbaa, M.; Ailam, E.H. Determination of the Complete Penetration Magnetic Field of a HTS Pellet from the Measurements of the Magnetic Field at its Top-Center Surface. *IEEE Trans. Appl. Supercond.* **2018**, *28*, 8800104.
22. Ginsberg, D.M. *Physical Properties of High Temperature Superconductor*; World Scientific, Singapore, 1988; 516p.
23. Durrell, J.H.; Dennis, A.R.; Jaroszynski, J.; Ainslie, M.D.; Palmer, K.G.; Shi, Y.H.; Campbell, A.M.; Hull, J.; Strasik, M.; Hellstrom, E.E.; et al. A trapped field of 17.6 T in melt-processed, bulk Gd-Ba-Cu-O reinforced with shrink-fit steel. *Supercond. Sci. Technol.* **2014**, *27*, 082001.

24. Masson, P.; Leveque, J.; Netter, D.; Rezzoug, A. Experimental study of a new kind of superconducting inductor. *IEEE Trans. Appl. Supercond.* **2003**, *13*, pp 2239-2242.
25. Netter, D.; Leveque, J.; Ailam, E.; Douine, B.; Rezzoug, A.; Masson, P.J. Theoretical study of a new kind HTS motor. *IEEE Trans. Appl. Supercond.* **2005**, *15*, 2186–2189.
26. Colle, A.; Lubin, T.; Ayat, S.; Gosselin, O.; Lévêque, J. Analytical Model for the Magnetic Field Distribution in a Flux Modulation Superconducting Machine. *IEEE Trans. Magn.* **2019**, *55*, pp. 1–9.
27. Tomita, M.; Murakami, M. High Temperature Superconductor Bulk Magnet that can trap magnetic fields of over 17 T at 29 K. *Nature* **2003**, *421*, 517–520.
28. Trillaud, F.; Berger, K.; Douine, B.; Lévêque, J. Comparaison between modeling and experimental results of magnetic flux trapped. *IEEE Trans. Appl. Supercond.* **2016**, *26*, 6800305.
29. Berger, K.; Gony, B.; Lévêque, B.D.J. Magnetization and Demagnetization Studies of an HTS Bulk in an Iron Core. *IEEE Trans. Appl. Supercond.* **2016**, *26*, 4700207.
30. Gony, B.; Berger, K.; Douine, B.; Koblishka, M.; Lévêque, J. Improvement of the Magnetization of a Superconducting Bulk using an Iron Core. *IEEE Trans. Appl. Supercond.* **2015**, *25*, 8801005.
31. Hirakawa, M.; Inadama, S.; Kikukawa, K.; Suzuki, E.; Nakasima, H. Developments of superconducting motor with YBCO bulk magnets. *Physica C* **2003**, *392–396*, pp. 773–776.
32. Shaanika, E.; Miki, M.; Bocquel, C.; Felder, B.; Tsuzuki, K.; Ida, T.; Izumi, M. Core Loss of a Bulk HTS Synchronous Machine at 2 and 3 T Rotor Magnetisation. *IEEE Trans. Appl. Supercond.* **2019**, *30*, 2927587.
33. Matsuzaki, H.; Kimura, Y.; Ohtani, I.; Izumi, M.; Ida, T.; Akita, Y.; Sugimoto, H.; Miki, M.; Kitano, M. An axial gap-type HTS bulk synchronous motor excited by pulsed-field magnetization with vortex-type armature copperwindings. *IEEE Trans. Appl. Supercond.* **2005**, *15*, 2222–2225.
34. Jiang, Y.; Pei, R.; Xian, W.; Hong, Z.; Coombs, T.A. The design, magnetization and control of a superconducting permanent magnet synchronous motor. *Supercond. Sci. Technol.* **2008**, *21*, 065011, doi:10.1088/0953-2048/21/6/065011.